Supporting Information

Table S1 Composition of trace elements in the synthetic influent.

Component	Concentration (mg/L)
$Na_2MoO_4 \cdot 2H_2O$	0.03
$FeSO_4 \cdot 7H_2O$	1
$CaCl_2 \cdot 2H_2O$	1
$MnCl_2 \cdot 4H_2O$	0.01
H_3BO_3	0.3
$ZnSO_4 \cdot 7H_2O$	0.1
$CoCl_2 \cdot 6H_2O$	0.2

Table S2 H_2-MBfR start-up and long-term operation parameter.

Parameter	Start-up phase				Stabilization Stage
	1–3	4–14	15–30	31–45	From 45 days onwards
H_2 pressure (MPa)	0.04	0.04	0.04	0.04	0.04
Influent flowrate (mL/min)	0	0.5	1	2	2
NO_3^--N Concentration (mg/L)	10	10	20	20	20
Recirculating flowrate (mL/min)	100	100	100	100	100
HRT (h)	24	21.6	10.8	5.9	5.9

Table S3 H_2-MBfR short-term operation parameter.

Reactors	Parameters	Periods		
R1: blank control R2:1 μg/L C_{14}-HSL R3:1 μg/L C_4-HSL	**Days of operation**	**1–3**	**3–20**	**20–65**
	H_2 pressure (MPa)	0	0.04	0.04
	Influent flowrate (mL/min)	0	0.5	1
	NO_3^--N Concentration (mg/L)	10	10	10
	Recirculating flowrate (mL/min)	100	100	100
	HRT (h)	24	21.6	10.8

S1 Signaling molecule detection

AHL concentrations were quantified using an HPLC-MS/MS assay (Waters I class-AB 5500, Waters, USA) with an electrospray ionization source and a BEH C18 column (2.1 mm × 100 mm with 1.7 μm particle size, Waters, USA) was set to 40℃. The mobile phase comprised 0.1% formic acid in water and methanol (Table S4). We selected 11 common AHLs as standards (from Sigma-Aldrich, HPLC, ≥ 95%, USA, Table S5) and used multiple reaction monitoring (MRM) for quantification and identity confirmation. Data were collected to construct standard curves from 0.5 to 50 μg/L, with linear calibration curves exhibiting high correlation coefficients (Fig. S1). The corresponding mass spectral conditions for the signal molecules are listed in Table S6.

Table S4 Mobile phase setting parameter table.

Time (min)	Mobile phase	
	A (%)	B (%)
0	70	30
1	70	30
3	10	90
6	10	90
6.1	70	30
7	70	30

Table S5 Classification of 11 common acyl homoserine lactones (AHLs).

Name	Abbreviations	Molecular Formula	Log P
N-butanoyl-homoserine lactone	C_4-HSL	$C_8H_{13}NO_3$	0.03
N-hexanoyl-homoserine lactone	C_6-HSL	$C_{10}H_{17}NO_3$	1.02
N-heptanoyl-homoserine lactone	C_7-HSL	$C_{11}H_{19}NO_3$	1.94
N-octanoyl-homoserine lactone	C_8-HSL	$C_{12}H_{21}NO_3$	1.97
N-decanoyl-homoserine lactone	C_{10}-HSL	$C_{14}H_{25}NO_3$	2.96
N-dodecanoyl-homoserine lactone	C_{12}-HSL	$C_{16}H_{29}NO_3$	4.02
N-tetradecanoyl-homoserine lactone	C_{14}-HSL	$C_{18}H_{33}NO_3$	5.09
N-3-oxo-ctanoyl-DL-homoserine lactone	3-oxo-C_8-HSL	$C_{12}H_{19}NO_4$	0.94
N-3-oxo-decanoyl-L-homoserine lactone	3-oxo-C_{10}-HSL	$C_{14}H_{23}NO_4$	1.70
N-3-oxy-dodecoacyl-L-homoserine lactone	3-oxo-C_{12}-HSL	$C_{16}H_{27}NO_4$	2.49
N-3-oxy-tedecyl-L-homoserine lactone	3-oxo-C_{14}-HSL	$C_{18}H_{31}NO_4$	3.35

Table S6 Mass spectrometry condition parameters corresponding to 11 signal molecules.

Name	Parent ion	Daughter ion	Collision voltage (V)	Declustering voltage (V)
C_4-HSL	172.8	102.1	12	70
C_6-HSL	200.1	102.1	13	70
C_7-HSL	214.1	102.1	15	70
C_8-HSL	228.1	102.1	14	70
C_{10}-HSL	256.1	102.1	15	70
C_{12}-HSL	284.2	102.1	16	70
C_{14}-HSL	312.2	102.1	12	70
3-oxo-C_8-HSL	242.1	102.1	15	70
3-oxo-C_{10}-HSL	270.1	102.1	16	70
3-oxo-C_{12}-HSL	298.2	102.1	16	70
3-oxo-C_{14}-HSL	326.2	102.1	18	70

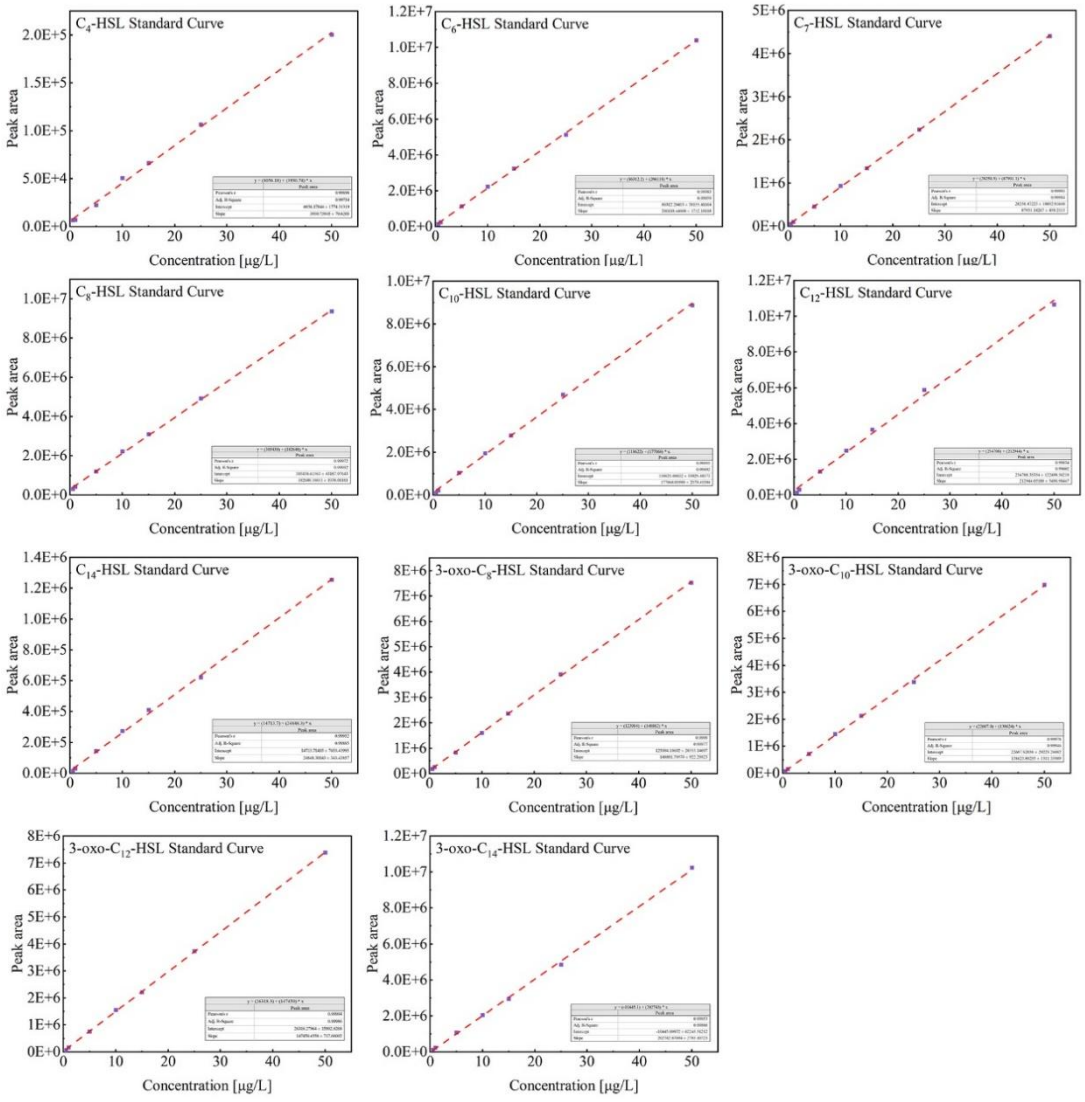

Fig. S1 Standard curves for 11 AHLs (Concentration range of 0.5 to 50 μg/L, $r \geq 0.998$).

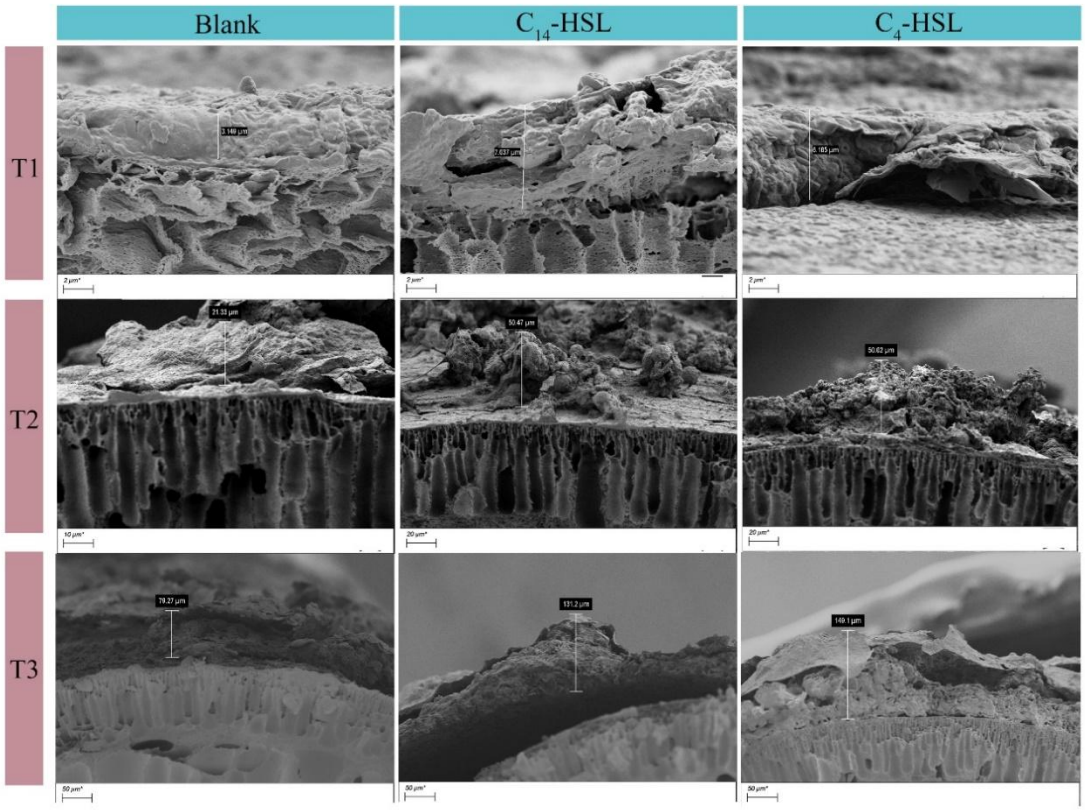

Fig. S2 Scanning electron microscopy (SEM) was employed to capture cross-sectional images of biofilms at various time intervals during short-term experiments. T1: 0–15 d, T2: 15–35 d, T3: 35–65 d. Biofilm samples were taken from the last day of each time period.

S2 Correlation analysis of H_2-MBfR microbial enrichment characteristics with AHLs

For the long-term experiments, Figs. S3(a) and S3(b) illustrate the top ten phyla and dominant genera in the biofilm at different operational stages. Phylum-level analyses (Fig. S3(a)) revealed that *Proteobacteria* (41.64%–64.81%) consistently dominated all the operational stages. Numerous studies have corroborated the presence of nitrogen-fixing bacteria within this phylum, which play a crucial role in the nitrogen transformation of wastewater (Chu et al., 2021; Jiang et al., 2022). The findings revealed a significant correlation between the majority of *Amoebacteria* and *Bacteroidetes* phyla, and quorum sensing (QS). This correlation is a crucial factor rendering this system invaluable for screening multiple AHLs. These results are consistent with those of the population-sensing genotype analysis of AHLs conducted by Sun et al. (2018).

Throughout the study, the reactor consistently hosted *Hydrogenophaga* (0.66%–1.71%), *Candidatus Accumulibacter* (0.55%–3.56%), and *Acidovorax* (0.57%–2.18%) at the genera level

(Fig. S3(b)) from the initial membrane hanging stage to the stabilization phase. *Hydrogenophaga*, a typical H_2 oxidizing bacterium (Jiang et al., 2020), is the primary denitrifying bacterium in numerous H_2-MBfR systems and plays a crucial role in nitrate removal (Zhao et al., 2011; Zhou et al., 2018; Xia et al., 2019). *Candidatus Accumulibacter*, identified as a denitrifying phosphorus-accumulating organism (DPAO), significantly contributes to denitrification by utilizing poly-β-hydroxy alkanoates (PHA) nutrients (Huang et al., 2020). *Acidovorax* is a mixed nutrient-driven denitrifying bacterium that can also reduce nitrate using H_2 as an electron donor (Blohm et al., 2022). A similar pattern was observed for *Thaura* (maximum 31.38%) (Long et al., 2018), which dominated the relative abundance during the rapid biofilm forming phase (day 30). This phase likely involved accelerated microbial film renewal metabolism, resulting in increased biomass production and greater fluctuations in increased biomass production and greater fluctuations in the *Proteobacteria* vs. *Euryarchaeota* ratio due to interspecific competition. Furthermore, *Methanobacterium*, a common methanogenic genus in *Euryarchaeota*, followed a trend similar to *Euryarchaeota* and accounted for a relatively higher proportion (12.32% compared to 3.23% on day 30) during the initial domestication phase. The other top ten relative abundances, *Mycobacterium*, *Nitrospira*, *Xanthobacter*, and *Azonexus*, demonstrated fluctuations throughout different periods and collectively participated in the denitrification process, maintaining the reactor in a high-denitrification state throughout the cycle.

To investigate the response of bacterial communities to AHL signals, the Pearson correlation coefficients between the top ten ranked genera and AHLs in the biofilm were compared (Fig. S3(c)). The results revealed a negative correlation between the abundance of genera that were highly ranked in the hydrogen-dependent denitrification system and most AHLs. Furthermore, a stronger negative correlation indicates a more rapid response of these genera to AHLs (Wang et al., 2021), suggesting the presence of widespread QS response mechanisms in this system. This negative feedback mechanism may increase in the abundance of certain genera. For instance, *Candidatus Accumulibacter* showed negative correlations with C_{14}-HSL and C_4-HSL (correlation coefficients of −0.48 and −0.45, respectively). The relative abundance of this genus increased by 0.40%–7.85% after the addition of C_{14}-HSL and by 0.10%–6.83% after the addition of C_4-HSL. Furthermore, C_4-HSL and C_{14}-HSL exhibited significant positive correlations with typical QS bacteria such as *Hydrogenophaga* and *Thaura* commonly found in wastewater treatment systems (Favre-Bonté et al., 2003; Wang et al., 2021). This suggests that these genera are major contributors to these two signaling molecules. The abundance of *Thaura* decreased by a maximum of 15.02% and 5.48% after the addition of C_{14}-HSL and C_4-HSL, respectively, whereas *Hydrogenophaga* decreased by a maximum of 8.8% and 6.33%, respectively. This indicates that the introduction of external AHLs may affect the response level of their own AHL-QS and may not always have a positive effect.

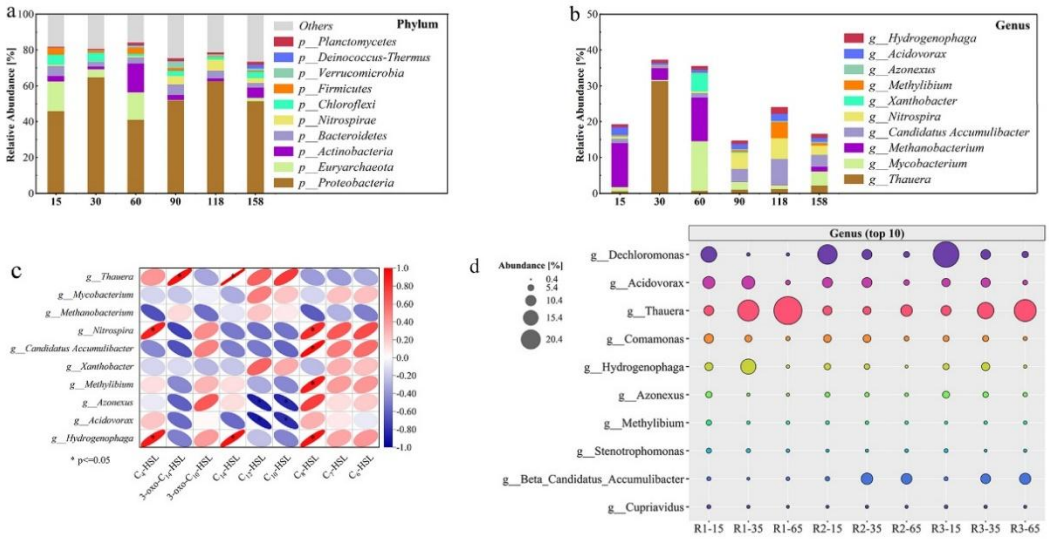

Fig. S3 Community (a) phylum level, (b) genus level in different stages of biofilm with relative abundance top ten, (c) correlation of the top ten bacterial groups in abundance with AHLs in long-term experiments, * represents $p \leqslant 0.05$, and (d) abundance of top ten genera in exogenous C_4-HSL and C_{14}-HSL experiments.

References

Blohm A, Kumar S, Knebl A, Herrmann M, Küsel K, Popp J, Frosch T (2022). Activity and electron donor preference of two denitrifying bacterial strains identified by Raman gas spectroscopy. Analytical and Bioanalytical Chemistry, 414(1): 601–611

Chu H, Liu X, Ma J, Li T, Fan H, Zhou X, Zhang Y, Li E, Zhang X (2021). Two-stage anoxic-oxic (A/O) system for the treatment of coking wastewater: Full-scale performance and microbial community analysis. Chemical Engineering Journal, 417: 129204

Favre-Bonté S, Köhler T, Van Delden C (2003). Biofilm formation by *Pseudomonas aeruginosa*: role of the C4-HSL cell-to-cell signal and inhibition by azithromycin. Journal of Antimicrobial Chemotherapy, 52(4): 598–604

Huang W, Gong B, He L, Wang Y, Zhou J (2020). Intensified nutrients removal in a modified sequencing batch reactor at low temperature: Metagenomic approach reveals the microbial community structure and mechanisms. Chemosphere, 244: 125513

Jiang L, Ji F, Liao Y, Mao Y, Shen Q, Zhuo Y, Zhang Q (2022). Denitrification performance and mechanism of denitrification biofilm reactor based on carbon-nitrate counter-diffusional. Bioresource Technology, 348: 126804

Jiang M, Zhang Y, Yuan Y, Chen Y, Lin H, Zheng J, Li H, Zhang X (2020). Nitrate removal and dynamics of microbial community of a hydrogen-based membrane biofilm reactor at diverse nitrate loadings and distances from hydrogen supply end. Water (Basel), 12(11): 3196–3208

Long M, Ilhan Z E, Xia S, Zhou C, Rittmann B E (2018). Complete dechlorination and mineralization of pentachlorophenol (PCP) in a hydrogen-based membrane biofilm reactor (MBfR). Water Research, 144: 134–144

Sun Y, He K, Yin Q, Echigo S, Wu G, Guan Y (2018). Determination of quorum-sensing signal substances in water and solid phases of activated sludge systems using liquid chromatography–mass spectrometry. Journal of Environmental Sciences-China, 69: 85–94

Wang N, Gao J, Liu Y, Wang Q, Zhuang X, Zhuang G (2021). Realizing the role of N-acyl-homoserine lactone-mediated quorum sensing in nitrification and denitrification: a review. Chemosphere, 274: 129970

Xia S, Xu X, Zhou L (2019). Insights into selenate removal mechanism of hydrogen-based membrane biofilm reactor for nitrate-polluted groundwater treatment based on anaerobic biofilm analysis. Ecotoxicology and Environmental Safety, 178: 123–129

Zhao H P, Van Ginkel S, Tang Y, Kang D W, Rittmann B, Krajmalnik-Brown R (2011). Interactions between perchlorate and nitrate reductions in the biofilm of a hydrogen-based membrane biofilm reactor. Environmental Science & Technology, 45(23): 10155–10162

Zhou L, Xu X, Xia S (2018). Effects of sulfate on simultaneous nitrate and selenate removal in a hydrogen-based membrane biofilm reactor for groundwater treatment: Performance and biofilm microbial ecology. Chemosphere, 211: 254–260